Hindawi Publishing Corporation
Advances in Condensed Matter Physics
Volume 2014, Article ID 370619, 6 pages
http://dx.doi.org/10.1155/2014/370619

Research Article

Determination of the DC Electrical Conductivity of Multiwalled Carbon Nanotube Films and Graphene Layers from Noncontact Time-Domain Terahertz Measurements

E. Dadrasnia,[1] H. Lamela,[1] M. B. Kuppam,[2] F. Garet,[2] and J.-L. Coutaz[2]

[1] *Optoelectronics and Laser Technology Group (GOTL), Carlos III de Madrid University, Leganes, 28911 Madrid, Spain*
[2] *IMEP-LAHC, UMR CNRS 5130, University of Savoy, 73376 Le Bourget du Lac Cedex, France*

Correspondence should be addressed to E. Dadrasnia; edadrasn@ing.uc3m.es

Received 22 January 2014; Accepted 15 March 2014; Published 7 April 2014

Academic Editor: Veer P. S. Awana

Measuring the DC conductivity of very thin films could be rather difficult because of the electrical contact issue. This DC conductivity can, however, be extracted from noncontact measurements at GHz and THz frequencies using elaborated conductivity models that nicely fit the experimental data. Here we employ this technique to study the DC conductivity of fragile nanometer-thick films of multiwalled carbon nanotubes and monolayer graphene. The THz response of the films is measured by THz time-domain spectroscopy. We show that the THz conductivity of the samples is well fitted by either Drude-Lorentz model or Drude-Smith model, giving information on the physics of electrical conductivity in these materials. This extraction procedure is validated by the good agreement between the so-obtained DC conductivity and the one measured with a classical 4-point probe in-line contact method.

1. Introduction

One-dimensional (1D) carbon nanotubes (CNTs) and two-dimensional (2D) graphene layers exhibit unique electrical, optical, and mechanical properties [1–3]. Consequently, these carbon nanostructures have been introduced in numerous electronic devices, such as field-effect transistors [4] and supercapacitors [5], or as conductive flexible adhesives [6]. A comprehensive knowledge of the electrical conduction in actual CNTs and graphene layers, as well as a precise measurement of its value, is compulsory for designing optimized electronic components. Commonly, contact devices are employed to characterize the current-voltage response of the carbon nanostructure samples and then to determine their electrical properties [7, 8]. However, the contacting issue may damage the fragile thin films and thus may prevent a multiple measurement procedure and/or a subsequent use of the tested devices. Therefore, a noncontact and nondestructive technique is needed in practice.

Among modern techniques, terahertz time-domain spectroscopy (THz-TDS) is known for years to be a precise tool for noncontact characterization of samples like semiconductor wafers [9], paint films [10], art and historical pieces [11], biological tissues [12], and so forth. Sub-THz continuous wave and THz-TDS have already been widely applied to study carbon nanostructure samples [13–15]. As THz-TDS delivers the magnitude and phase of the THz waves transmitted or reflected by the samples, the complex permittivity of the sample material is obtained from THz-TDS data. In the case of conductive materials, the THz conductivity can be calculated from the complex permittivity. However, the DC conductivity cannot be directly determined, as the available THz power decreases sharply and falls below the noise level at lower frequencies (typically below 100 GHz). Nevertheless, by fitting the experimental THz-TDS data with an adequate conductivity model, the electrical conductivity can be extrapolated from its measured values at THz frequencies, assuming the material does not exhibit resonances at lower frequencies, like piezoelectric ones. As compared to free space measurements at lower frequencies (MHz-GHz), working at THz frequencies exhibits the strong advantage of a smaller wavelength, which permits dealing

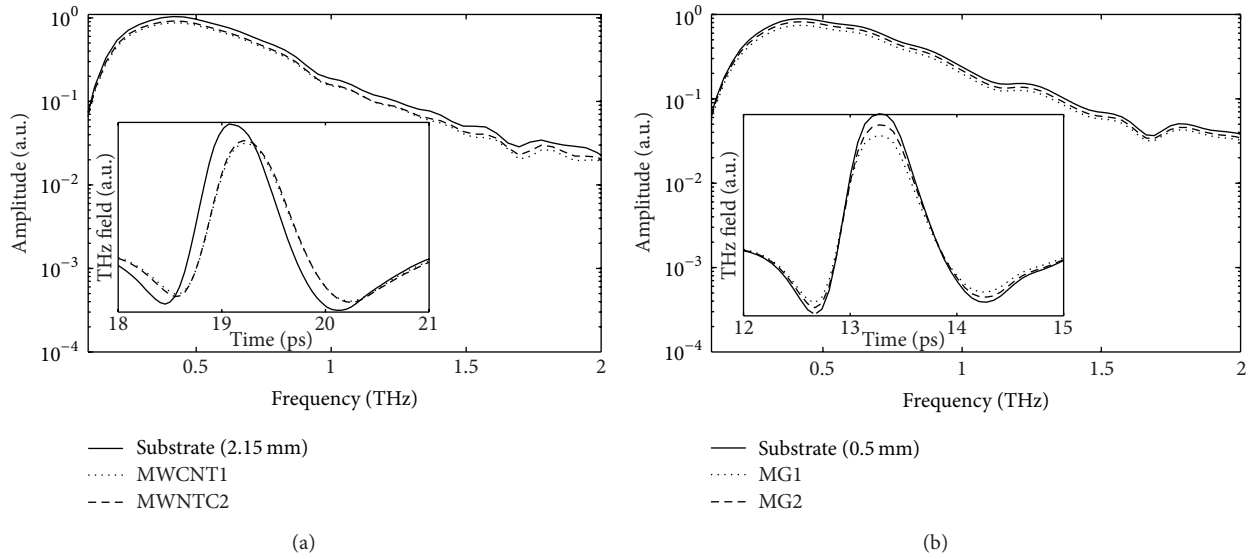

Figure 1: THz spectra obtained for (a) MWCNT samples and (b) MG samples. Insets show the corresponding temporal signal achieved.

with smaller realistic samples without artifact induced by diffraction effects.

In this work, we apply this procedure to obtain the electrical DC conductivity of multiwalled carbon nanotubes (MWCNTs) films and of monolayer pristine graphene (MG) samples. The conductivities of the MWCNT and MG samples are, respectively, described with a combined Drude and Lorentz model and by a Drude-Smith model. To validate our procedure, we compare the so-achieved DC conductivities with the ones obtained with a conventional 4-point probe measurement [16]. The good agreement demonstrates the efficiency of the noninvasive THz-TDS technique in determining the electrical parameters of fragile thin films [17–20].

2. Experimental Part

2.1. MWCNT and MG Samples. MWCNT samples were made of a pure and homogenous thin film of MWCNTs deposited over a fused quartz substrate. A nanotube suspension was prepared by mixing and ultrasonicating (380 W, 20 min) deionized water (10 mL), sodium dodecyl sulfate (Sigma Aldrich 71725, 0.1 g), and MWCNTs (Hanwha Nanotech CMP-330F, 10 mg). The nanotube suspension was deposited on a filter paper (Whatman Anodisc 25) by the vacuum filtration method. Then, we removed the sodium dodecyl sulfate surfactant by rinsing with deionized water. Finally, the MWCNTs films were transferred onto fused quartz substrates. The MWCNTs film thickness of our two samples, namely, MWCNT1 and MWCNT2, is 162 and 193 nm, respectively. The diameter of the films is 18 mm, while the quartz substrate is a $25 \times 25 \times 2.15\,\text{mm}^3$ [13].

MG films were fabricated as follows [2, 21]: copper foils from Alfa Aesar (46986, 99.8%, thickness 25 μm) were used as catalytic substrates. They were heated to 1000°C with H2 flow (3 sccm) and annealed at 1000°C for 30 min. Then, graphene films were grown by a low pressure chemical vapor deposition (LPCVD) by introducing CH4 in the deposition chamber for 10 min (20 sccm). Specimens were lastly cooled rapidly to room temperature, without any gas flow. The synthesized MG films were transferred onto a fused quartz substrate ($20 \times 20 \times 0.5\,\text{mm}^3$) by the wet transfer method. A thin layer of polymethyl methacrylate (PMMA) dissolved in chlorobenzene (Sigma-Aldrich 82265, 46 mg/mL) was put on top of MG, followed by a curing. Then, the copper substrate was etched in ammonium peroxydisulfate solution (Alfa Aesar 54106, ACS, 98.0%, 0.1 M) for 3 hours. Finally, the PMMA/graphene film was transferred onto the fused quartz substrate, followed by removal of PMMA using acetone. The MG film thickness of our two samples, namely, MG1 and MG2, is a one-atom thick layer deposit on over quartz substrates ($15 \times 15 \times 0.5\,\text{mm}^3$). Fused quartz was chosen as the substrate material for all samples because of its high transparency in the THz domain (Figure 1). It exhibits a refractive index of about 1.95 and its power absorption is low but increases continuously with frequency to reach 8 cm^{-1} at 2 THz (inset of Figure 2).

2.2. Time-Domain Spectroscopy and THz Signals. The THz responses of the samples have been characterized using a conventional THz-TDS setup [22, 23]. The samples are located at the waist of the THz beam: at any frequency of the available THz signal, the Rayleigh length of the beam is much larger than the bare or covered substrate; therefore, the sample can be considered as illuminated at normal incidence by a plane wave. To execute a THz differential analysis, 3 measurements have been performed for each sample: one without sample, one with a bare substrate, and finally one with the MWCNT (Figure 1(a)) and MG (Figure 1(b)) samples.

The waveforms are recorded over a 35 ps time window, leading to a spectral resolution of 28 GHz. Each waveform has been recorded several times, in order to check the experimental reproducibility and to minimize the noise by

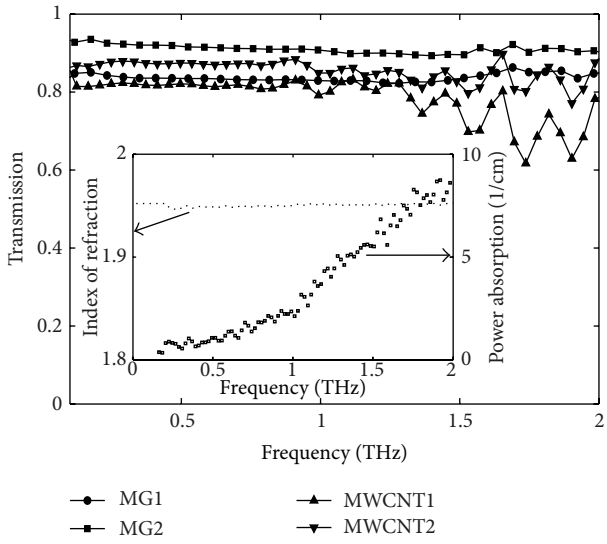

Figure 2: THz pulses transmitted through MWCNT and MG samples. The inset shows the optical properties of noncovered fused quartz at THz frequencies.

averaging the records. The THz spectrum of the averaged waveforms is obtained through a numerical fast Fourier transform. To simplify the extraction of the film parameters, an appropriate time windowing of the substrate and sample waveforms rejects the echoes resulting from rebounds in the substrate [24].

Under this hypothesis, the frequency signals write

$$S_S(\omega) = S_o t_{as} t_{sa} e^{j(\omega/c)d} e^{j(\omega/c)\tilde{n}_s D},$$
$$S_F(\omega) = S_o \frac{t_{af} t_{fs} t_{sa}}{1 - r_{fs} r_{fa} e^{j2(\omega/c)d\tilde{n}_f}} e^{j(\omega/c)d\tilde{n}_f} e^{j(\omega/c)\tilde{n}_s D}, \quad (1)$$

where the subscripts S and F designate the signals measured, respectively, for bare substrate and covered substrates. S_o is the air-incident beam. The subscripts a, f, and s are for ambient medium (air), film, and substrate. d is the thickness of the MG sample; t_{ij} and r_{ij} are the coefficients of transmission and reflection at the interface between media i and j. $\tilde{n}_i = n_i + j\kappa_i$ is the complex refractive index of medium i. From (1), the complex transmission $T(\omega)$ for thin film with magnitude (ρ) and phase shift (ϕ) can be defined as

$$T(\omega) = \frac{S_F(\omega)}{S_S(\omega)} = \rho(\omega) e^{i\phi(\omega)}. \quad (2)$$

3. Models for THz Conductivity

In MWCNT thin films, both free electrons, moving along a nanotube or from a nanotube to another one, and bound electrons, through resonant oscillations, contribute to the relative permittivity. In addition, the free conductivity of the CNTs depends on how the CNTs are rolled into [25]. Low-frequency phonon modes, that are resonant at THz frequencies, are strongly involved in carrier scattering [26]. Thus, it is necessary to combine both Drude approach of metallic conductivity and Lorentz model of dielectric permittivity to describe the electromagnetic response of MWCNTs. Moreover, the films consist of random and nonaligned tubes dispersed in air, but with dimensions much smaller than the THz wavelength. Thus, from an electromagnetic point of view, the MWCNT film can be treated as an effective medium with a complex permittivity function $\tilde{\varepsilon}_{\text{eff}}$ [27]. Taking into account the involved contributions to the permittivity, we write

$$\tilde{\varepsilon}_{\text{eff}} = \varepsilon_\infty + \sum_{k=0}^{K} \frac{f_k \omega_p^2}{\omega_k^2 - \omega^2 + j\omega\Gamma_k}, \quad (3)$$

where ω_p, ω_k, f_k, and Γ_k are, respectively, the plasma frequency, the resonance frequency, the strength, and the damping frequency of the kth mode.

On the other hand, a graphene film is a homogeneous conducting material. The plasma frequency and carrier density have a nonlinear dependency, because of the conical dispersion of the energy with momentum. It is important to note that, in the THz range, absorption through intraband transitions dominates the one related to interband transitions [28], and thus intraband absorption influences mainly the THz conductivity. Therefore, up to date, THz conductivity of graphene films has been fitted using the Drude model [29]. However, we will show here that the Drude model as modified by Smith [30], taking into account a nonrandom scattering of the free carriers, allows one to better adjust the experimental data with the modeled curve. In the Drude-Smith (DS) model, the expression of the complex conductivity is

$$\tilde{\sigma}(\omega) = \frac{\sigma_{\text{DC}}}{1 - i\omega\tau} \left(1 + \sum_{m=1}^{\infty} \frac{c_m}{(1 - i\omega\tau)^m}\right), \quad (4)$$

where the c_m coefficient is the fraction of the electron original velocity that is retained after the mth collision. If $c_m = 0$, the carrier momentum is totally randomized (classical model by Drude). If $c_m = -1$, the free carrier is completely backscattered [31].

4. Results and Discussion

Figure 2 presents the transmission spectrum of the different studied samples as determined from the experimental data using relation (2). All samples show almost a steady state transmission line up to 1.5 THz. However, afterwards there are fluctuations due to the insufficient THz power. MG2 and MWCNT2 are, respectively, the most (~94%) and least (~81%) transparent samples.

4.1. MWCNT Samples. The imaginary part of the permittivity of the films, to which the absorption of the electromagnetic wave is related, is in turn proportional to the real part of the electrical conductivity. Figure 3(a) depicts the THz real conductivity of the films: it monotonically increases with increasing frequency for both MWCNT samples. Figure 3(b) shows the imaginary part of the electrical conductivity, which

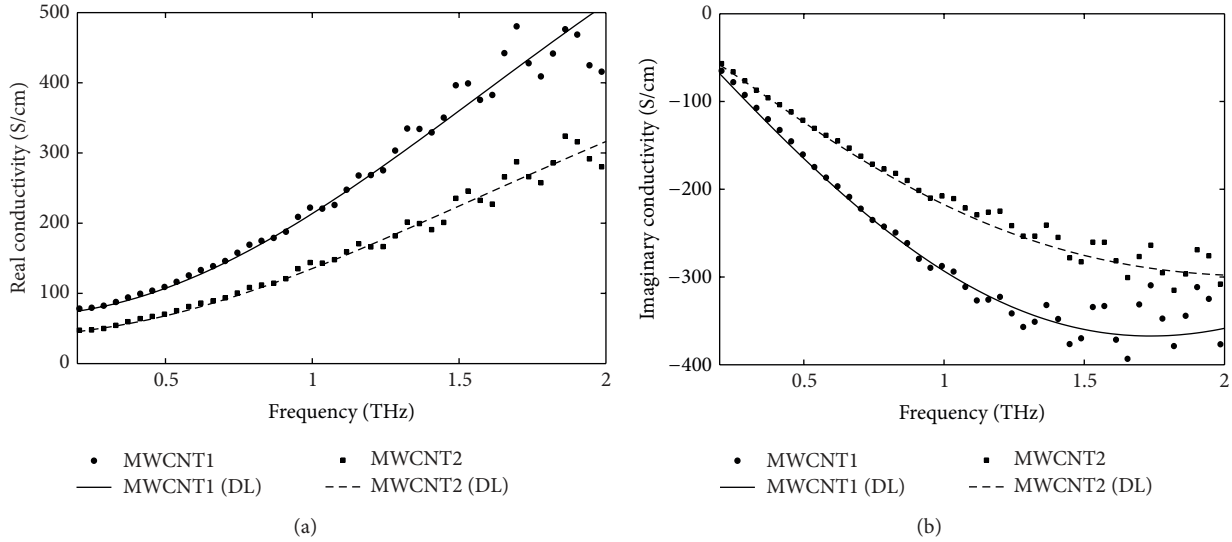

Figure 3: (a) Real and (b) imaginary parts of measured (markers) and fitted DL model (lines) results of electrical conductivity for MWCNT samples.

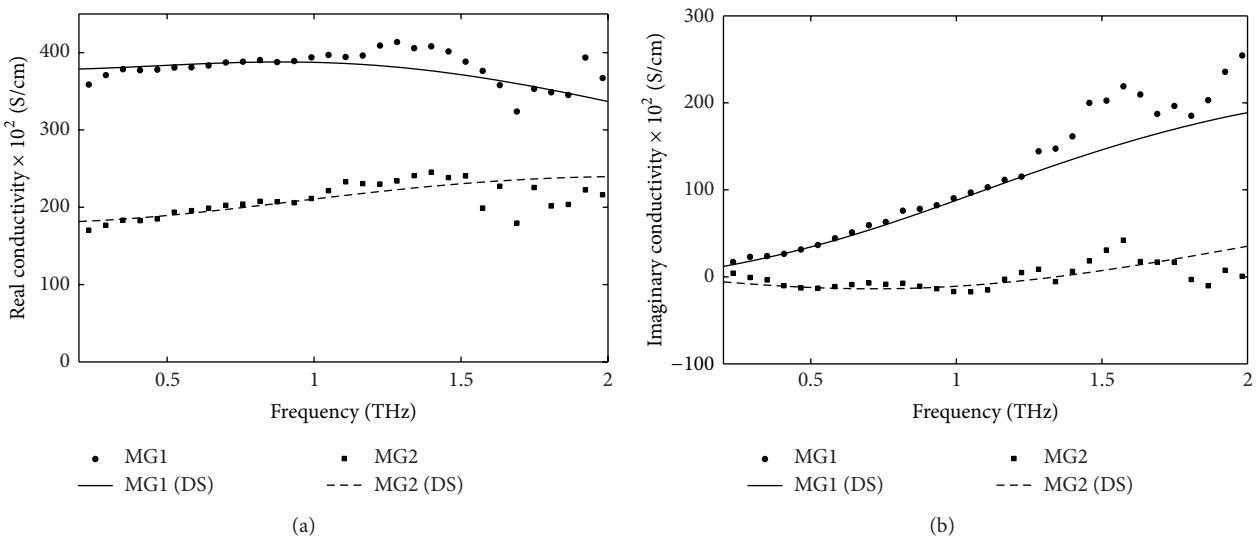

Figure 4: (a) Real and (b) imaginary parts of measured (markers) and fitted DS model (lines) results of electrical conductivity for MG samples.

decreases with increasing frequency. Then, the conductivity does not follow the simple Drude model and we need to consider the Lorentzian contribution at high frequencies as mentioned in (3). Our fits of the experimental data are plotted as lines in Figures 3(a) and 3(b). One can notice the excellent agreement between measured and calculated conductivities, in both cases of real and imaginary parts. The so-achieved plasma frequency is $f_p = \omega_p/2\pi \approx 45$ THz, corresponding to an equivalent-bulk density of carriers of $2\text{–}4 \times 10^{19}$ cm^{-3}. Thus, this plasma frequency of MWCNT films is much higher than the one in semiconductors [32] and smaller than in metals [31] with a scattering time ($\tau \approx 10$ fs) of the order of metallic materials. In regular semiconductors, f_p is proportional to the square root of carrier density and inversely proportional to the effective mass of the carriers. The average effective electron mass and electron carrier density of MWCNTs are found between the ones of doped semiconductors (e.g., n-doped silicon) and perfect metal (e.g., Au). This behavior depends on physical structure and varying chiral vector indices of the tubes. The Lorentz resonance frequency is around 4 and 6 THz, respectively, for MWCNT1 and MWCNT2.

4.2. MG Samples. Figures 4(a) and 4(b) display the THz conductivity of MG samples. MG1 real conductivity is twice the one of MG2, while its imaginary part is much higher. The values of conductivity are known to be sensitive to the thickness of the MG films [14]. This difference in conductivity behavior of the studied MG samples could come from the slight variation in the transfer during the CVD synthesis

Table 1: DC conductivity obtained using 4-probe technique and determined from THz Drude models.

Samples	4-Probe conductivity (S/cm)	THz-Drude conductivity (S/cm)
MWCNT1	70.6	70.7
MWCNT2	66.6	66.7
MG1	3.46×10^4	3.5×10^4
MG2	6.96×10^3	2.1×10^4

process. Also, MG2 shows a non-Drude response because of its smaller area than MG1, which explains why the conductivity shows an oscillator at higher frequencies. As a result of large scattering rates, the studied spectral range is below the Drude roll-off frequency. For the MG1 sample, both real and imaginary parts of conductivity increase with increasing frequency, which is well fitted by a Drude-like form ($c_m = 0$, $f_p \approx 571$ THz and $\tau = 34$ fs) of the frequency-dependent conductivity [18]. For the MG2 sample, however, the negative imaginary part of THz conductivity decreases with increasing frequency. It cannot be explained by a simple Drude model, but it is well described by the Drude-Smith theory (relation (4)) with $m = 1$ and $c_1 = -0.6$. The large negative value of c_1 indicates that the electrons are affected by backward scattering as a result of the structural disorder effects in graphene [14]. As for MG1 samples, the plasma frequency $f_p \approx 492$ THz is in the visible range while the collision value ($\tau = 53$ fs) is comparable to the ones of metals.

4.3. Samples DC Conductivity. THz-TDS setups do not offer enough signal-to-noise ratio to determine the precise conductivity at low frequencies, because the efficiency of their dipole-like THz antennas vanishes when reaching the DC regime. However, this information can be extrapolated from the conductivity by fitting the spectra over the whole THz range, which minimizes the effect of noise or of discrepancies at some given frequencies. The DC conductivity of the films is simply deduced from the permittivity constant at frequency $\omega = 0$, using the fitted plasma frequency and collision time ($\sigma_{DC} = \omega_p^2 \tau \varepsilon_0$). The so-obtained values are given in the third column of Table 1.

To validate our method, the DC electrical conductivity of the films was measured with a classical 4-probe technique, using a Keithley 6221 current source and a Keithley 2182A nanovoltmeter. Even though the 4-probe technique is always difficult to implement when dealing with thin films (the probes may mechanically damage the film at the contact location), the measured DC conductivity (column 2 of Table 1) is very close to the average values deduced from THz-TDS measurements and conductivity models (column 3 of Table 1). There is only one disagreement related to sample MG2. It could arise from the not perfect fit of the conductivity curve at lower frequency (Figure 4) and especially of the imaginary part of the conductivity, which is too small to be determined with a great precision.

5. Conclusion

To summarize, THz-TDS has been demonstrated to be a powerful noncontact tool to study the electrical conductivity of MWCNT and MG films from DC to THz frequencies. The whole spectrum analysis gives us reliable information for the DC electrical characterization of the samples. The conductivity of the films was extracted from THz-TDS data using-combined Drude models. The agreement between measured and fitted values is good, even though the experimental values were rather noisy due to thickness of thin films compared to the thick substrates and also the limited sensitivity of the THz-TDS setup over 1.5 THz.

The electrical conductivity of MG films with zero bandgap is almost three orders of magnitude at DC level and two orders of magnitude at THz frequencies, larger than the one of MWCNT films. MWCNT conductivity indeed depends on the crystallinity of the graphitic layers and the number of surface defects. MG1 and MG2 conductivities are well described by Drude and non-Drude models. The backward scattering occurring in the free electron movement may be explained by the structural disorder of the MG2 film Drude-Smith response.

Conflict of Interests

The authors declare that there is no conflict of interests regarding the publication of this paper.

Acknowledgment

This work was supported by the European Commission (Project 238393 ITN-FP7 MITEPHO, "Microwave and Terahertz Photonics").

References

[1] Z. Wu, Z. Chen, X. Du et al., "Transparent, conductive carbon nanotube films," *Science*, vol. 305, no. 5688, pp. 1273–1276, 2004.

[2] S. Bae, H. Kim, Y. Lee et al., "Roll-to-roll production of 30-inch graphene films for transparent electrodes," *Nature Nanotechnology*, vol. 5, no. 8, pp. 574–578, 2010.

[3] P. R. Bandaru, "Electrical properties and applications of carbon nanotube structures," *Journal of Nanoscience and Nanotechnology*, vol. 7, no. 4-5, pp. 1239–1267, 2007.

[4] H. R. Byon and H. C. Choi, "Network single-walled carbon nanotube-field effect transistors (SWNT-FETs) with increased schottky contact area for highly sensitive biosensor applications," *Journal of the American Chemical Society*, vol. 128, no. 7, pp. 2188–2189, 2006.

[5] D. Yu and L. Dai, "Self-assembled graphene/carbon nanotube hybrid films for supercapacitors," *Journal of Physical Chemistry Letters*, vol. 1, no. 2, pp. 467–470, 2010.

[6] R. Ma, S. Kwon, Q. Zheng et al., "Carbon-nanotube/silver networks in nitrile butadiene rubber for highly conductive flexible adhesives," *Advanced Materials*, vol. 24, no. 25, pp. 3344–3349, 2012.

[7] T. W. Ebbesen, H. J. Lezec, H. Hiura, J. W. Bennett, H. F. Ghaemi, and T. Thio, "Electrical conductivity of individual carbon nanotubes," *Nature*, vol. 382, no. 6586, pp. 54–56, 1996.

[8] P. L. McEuen and J.-Y. Park, "Electron transport in single-walled carbon nanotubes," *MRS Bulletin*, vol. 29, no. 4, pp. 272–242, 2004.

[9] D. M. Mittleman, J. Cunningham, M. C. Nuss, and M. Geva, "Noncontact semiconductor wafer characterization with the terahertz Hall effect," *Applied Physics Letters*, vol. 71, no. 1, pp. 16–18, 1997.

[10] T. Yasui, T. Yasuda, K.-I. Sawanaka, and T. Araki, "Terahertz paintmeter for noncontact monitoring of thickness and drying progress in paint film," *Applied Optics*, vol. 44, no. 32, pp. 6849–6856, 2005.

[11] J. Labaune, J. B. Jackson, S. Pagès-Camagna, I. N. Duling, M. Menu, and G. A. Mourou, "Papyrus imaging with terahertz time domain spectroscopy," *Applied Physics A: Materials Science and Processing*, vol. 100, no. 3, pp. 607–612, 2010.

[12] E. Castro-Camus, M. Palomar, and A. A. Covarrubias, "Leaf water dynamics of *Arabidopsis thaliana* monitored *in-vivo* using terahertz time-domain spectroscopy," *Scientific Reports*, vol. 3, article 2910, 2013.

[13] S. Puthukodan and E. Dadrasnia, "Sub-THz characterization of multiwalled carbon nanotube thin films using a vector network analyzer," *Electronics Letters*, vol. 50, no. 4, pp. 297–299, 2014.

[14] X. Zou, J. Shang, J. Leaw et al., "Terahertz conductivity of twisted bilayer graphene," *Physical Review Letters*, vol. 110, Article ID 067401, 2013.

[15] E. Dadrasnia, H. Lamela, M.-B. Kuppam, F. Garet, and J.-L. Coutaz, "THz time-domain spectroscopy in different carbon nanotube thin films," in *Terahertz Technology and Applications V*, vol. 8261 of *Proceedings of SPIE*, San Francisco, Calif, USA, January 2012.

[16] K.-Y. Chun, Y. Oh, J. Rho et al., "Highly conductive, printable and stretchable composite films of carbon nanotubes and silver," *Nature Nanotechnology*, vol. 5, no. 12, pp. 853–857, 2010.

[17] E. P. J. Parrott, J. A. Zeitler, J. McGregor et al., "The use of terahertz spectroscopy as a sensitive probe in discriminating the electronic properties of structurally similar multi-walled carbon nanotubes," *Advanced Materials*, vol. 21, no. 38-39, pp. 3953–3957, 2009.

[18] J. T. Hong, K. M. Lee, B. H. Son et al., "Terahertz conductivity of reduced graphene oxide films," *Optics Express*, vol. 21, no. 6, pp. 7633–7640, 2013.

[19] J. L. Tomaino, A. D. Jameson, J. W. Kevek et al., "Terahertz imaging and spectroscopy of largearea single-layer graphene," *Optics Express*, vol. 19, no. 1, pp. 141–146, 2011.

[20] Z. Wu, L. Wang, Y. Peng, A. Young, S. Seraphin, and H. Xin, "Terahertz characterization of multi-walled carbon nanotube films," *Journal of Applied Physics*, vol. 103, no. 9, Article ID 094324, 2008.

[21] X. Li, Y. Zhu, W. Cai et al., "Transfer of large-area graphene films for high-performance transparent conductive electrodes," *Nano Letters*, vol. 9, no. 12, pp. 4359–4363, 2009.

[22] H. Lamela, E. Dadrasnia, D. -M. Lee et al., "Terahertz conductivity studies in carbon nanotube networks prepared by the vacuum filtration method," in *Carbon Nanotubes, Graphene, and Associated Devices V*, vol. 8462 of *Proceedings of SPIE*, San Diego, Calif, USA, August 2012.

[23] E. Dadrasnia, S. Puthukodan, and H. Lamela, "Terahertz electrical conductivity and optical characterization of composite nonaligned single- and multiwalled carbon nanotubes," *Journal of Nanophotonics*, vol. 8, no. 1, pp. 083099–083099, 2014.

[24] L. Duvillaret, F. Garet, and J.-L. Coutaz, "A reliable method for extraction of material parameters in terahertz time-domain spectroscopy," *IEEE Journal on Selected Topics in Quantum Electronics*, vol. 2, no. 3, pp. 739–745, 1996.

[25] M. J. O. Connell, *Carbon Nanotubes Properties and Applications*, CRC Press/Taylor & Francis Group, Boca Raton, Fla, USA, 2006.

[26] S. Kumar, N. Kamaraju, A. Moravsky et al., "Terahertz time domain spectroscopy to detect low-frequency vibrations of double-walled carbon nanotubes," *European Journal of Inorganic Chemistry*, no. 27, pp. 4363–4366, 2010.

[27] T. Yamabe, K. Fukui, and K. Tanaka, *The Science and Technology of Carbon Nanotubes*, Elsevier, San Diego, Calif, USA, 1999.

[28] B. Sensale-Rodriguez, Y. Rusen, L. Lei, D. Jena, and H. G. Xing, "Graphene for reconfigurable terahertz optoelectronics," *Proceedings of the IEEE*, vol. 101, no. 7, pp. 1705–1716, 2013.

[29] J. T. Hong, K. M. Lee, B. H. Son et al., "Terahertz conductivity of reduced graphene oxide films," *Optics Express*, vol. 21, no. 6, pp. 7633–7640, 2013.

[30] N. V. Smith, "Classical generalization of the Drude formula for the optical conductivity," *Physical Review B: Condensed Matter and Materials Physics*, vol. 64, no. 15, Article ID 155106, 2001.

[31] J. Lloyd-Hughes and T. I. Jeon, "A review of the terahertz conductivity of bulk and nano-materials," *Journal of Infrared, Millimeter, and Terahertz Waves*, vol. 33, no. 9, pp. 871–925, 2012.

[32] T.-I. Jeon and D. Grischkowsky, "Nature of conduction in doped silicon," *Physical Review Letters*, vol. 78, no. 6, pp. 1106–1109, 1997.